Nanotechnology and Nano-Interface Controlled Electronic Devices
Editors: M. Iwamoto, K. Kaneto and S. Mashiko

CHAPTER 13

Structural color forming system composed of polypeptide-based LB films

Takatoshi Kinoshita [a], Shujiro Hayashi [b], Yoshiyuki Yokogawa [b], and Shintaro Washizu [c]

[a] *Department of Materials Science and Engineering, Nagoya Institute of Technology, Gokiso-cho, Showa-ku Nagoya 466-8555, Japan*
E-mail: kinosita@mse.nitech.ac.jp
[b] *National Institute of Advanced Industrial Science and Technology, Hirate-cho 1-1, Kita-ku, Nagoya 462-8510, Japan*
[c] *Fujinomiya Research Laboratories, Fuji Photo Film co., LTD., Fujinomiya Shizuoka 418-8666, Japan*

1. Introduction

Fig. 1 shows an example of an intelligent function of a living system. Living cells sense their environment as a stimulus and respond to environmental changes for the maintenance of life. For example, a physical or chemical stimulus is accepted by the signaling cell and the induced signal is transmitted to the nerve system with a nerve impulse, and finally, to the muscle cell with an accompanying contraction as response. One of the important points for us was that these sensory systems are installed at biological interfaces such as the biological membranes.

30 years ago, Singer and Nicolson [1] predicted that biological membranes are an assembly of molecular machines, each responsible for an elementary function. This idea has been reasonably accepted now. And it is recognized that the biological membranes are a self-organized system composed of amphiphilic molecules such as lipids and membrane proteins, and the specific location and/or molecular orientation of these elements are essential to lead the intelligent functions at the biological interfaces.

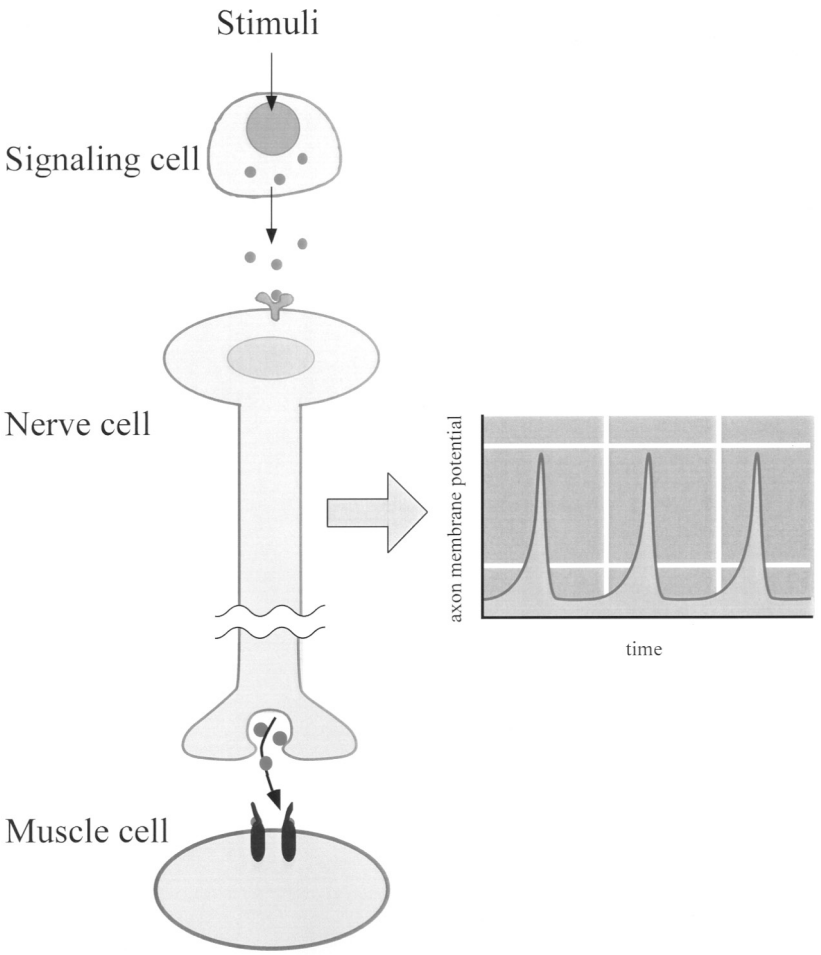

Fig. 1: Transmembrane signaling and sensation.

As a part of the membrane mimetic chemistry or supramolecular science, monolayer, bilayers and vesicles have been extensively studied using lipid-like amphiphiles, and more recently, the formation of molecular membrane systems composed of α-helical polypeptides is also investigated.

For example, Kimura et al. [2] reported on a α-helix regularly standing system as a self-assembled monolayer (SAM) on Au substrate (Fig. 2). Higashi et al. [3] showed the preparation of a α-helix rich PLGA monolayer and its enantioselectivety.

For the last few years, we [4] have tried to construct novel artificial membrane or interfacial systems using polypeptides and their derivatives as a very simple model polymer of membrane proteins. And at the same time we proposed two approaches for mimicking the intelligent functions of biological membrane systems (Fig. 3). One is functional modeling such as stimulus–response coupling, information transfer, and so

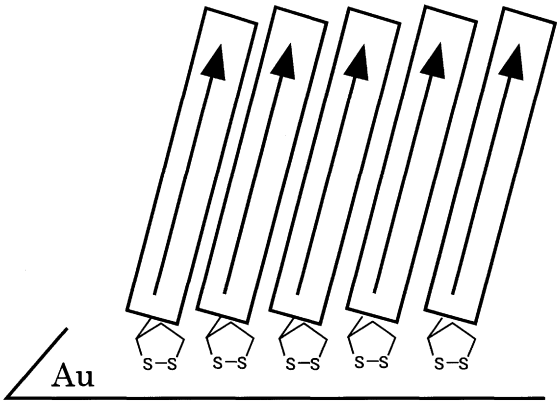

Fig. 2: Schematic illustration of a SAM of a helical peptide.

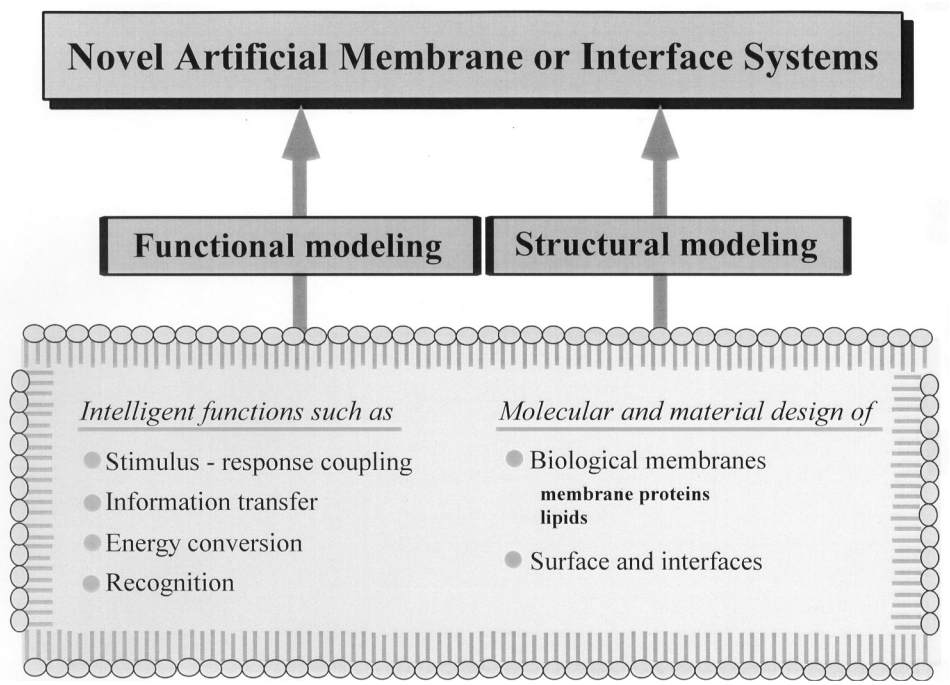

Fig. 3: A fundamental concept for mimicking biological membranes and interfaces.

on. The other is structural modeling, i.e., mimicking the design of biological membrane components such as membrane proteins and the surface and/or interface structure of living systems. Based on this concept, we will show here two types of polypeptide membrane systems (Fig. 4). One is the self-organized two-dimensional patterning in an amphiphilic helix monolayer. And the other is the polypeptide Langmuir–Blodgett (LB)

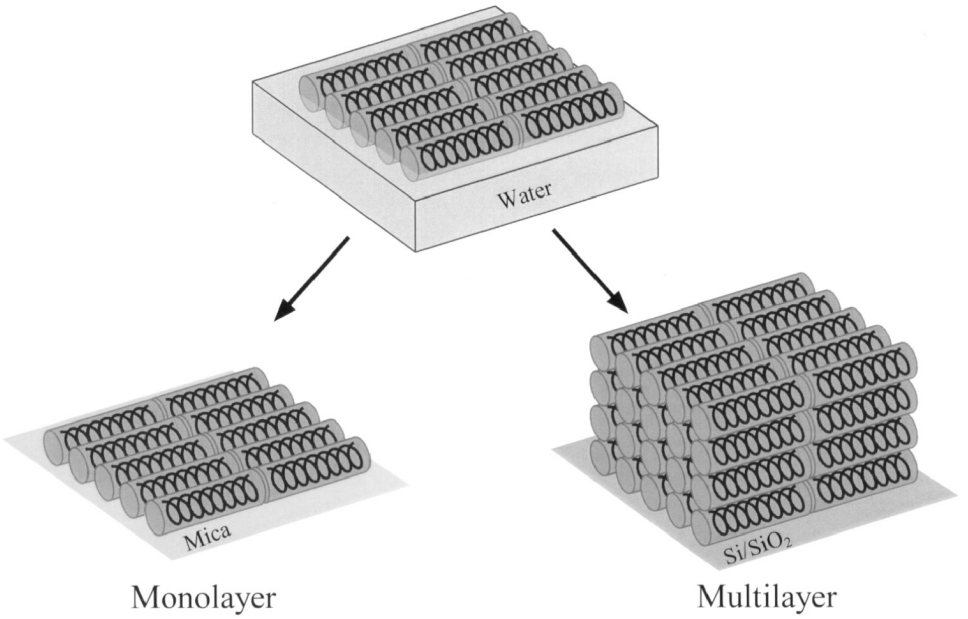

Fig. 4: Molecular membrane system composed of α-helical polypeptide.

film. For the former topic, we will show a possibility of nanometer-scale control of two-dimensional structure. And for the latter, structural color formation and regulation will be shown.

2. Self-organized two-dimensional patterning by α-helical block-copolypeptides

A monolayer was firstly prepared by a diblock-copolypeptide composed of hydrophilic and hydrophobic α-helix segments [5]. The hydrophobic segment is poly(L-lysine) derivative and the hydrophilic segment is L-glutamic acid copolymer. The stable α-helix structure was confirmed by circular dichroism measurement of the TFE solution of the polymer. So this polymer, as schematically shown in Fig. 5, is composed of a hydrophobic larger-diameter helix and a smaller-diameter and longer hydrophilic helix rod.

The monolayer was prepared by spreading a DMF/benzene mixed solution of the polymer on a water surface at pH 5 (Fig. 6). And the surface pressure was monitored by compressing the monolayer by the Wilhelmy method.

Fig. 7 shows the surface pressure–area isotherm obtained at pH = 5. The limiting area was estimated to be ca. 6 nm^2/molecule. The calculated limiting area when the helix is normal to the air/water interface is shown in Table 1. We expected the normal orientation of the helix after compressing the membrane, however, the big difference between the calculated and observed limiting area indicated that it is impossible to obtain a standing helix monolayer using this system.

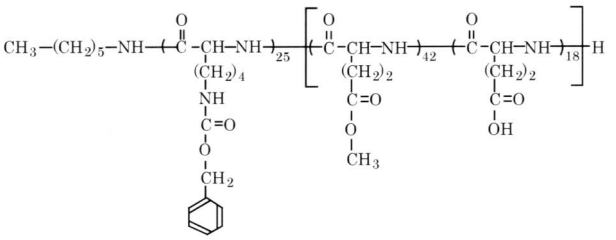

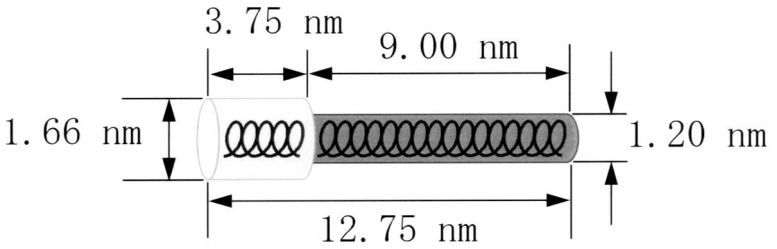

Fig. 5: Chemical structure and schematic illustration of $PLLZ_{25}$–$P(MLG_{42}/LGA_{18})$ (poly(ε-benzyloxycarbonyl L-lysine)$_{25}$–poly[(γ-methyl L-glutamate)$_{42}$/(L-glutamic acid)$_{18}$]).

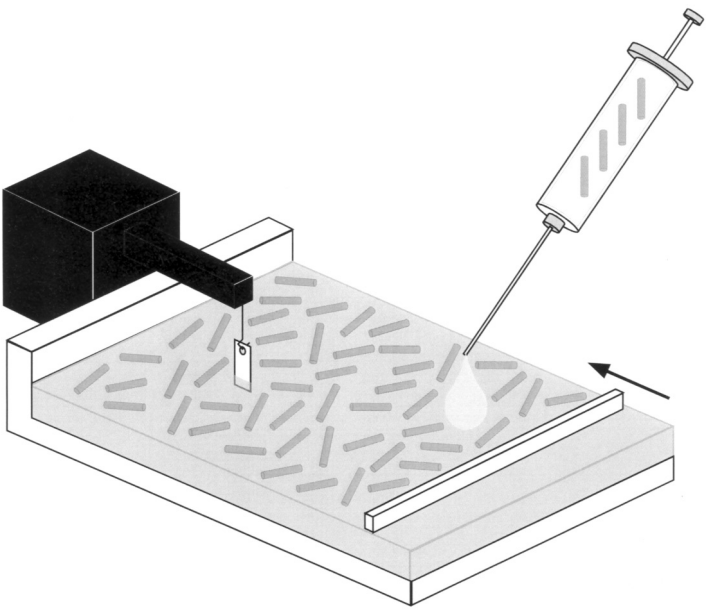

Fig. 6: Surface pressure measurements.

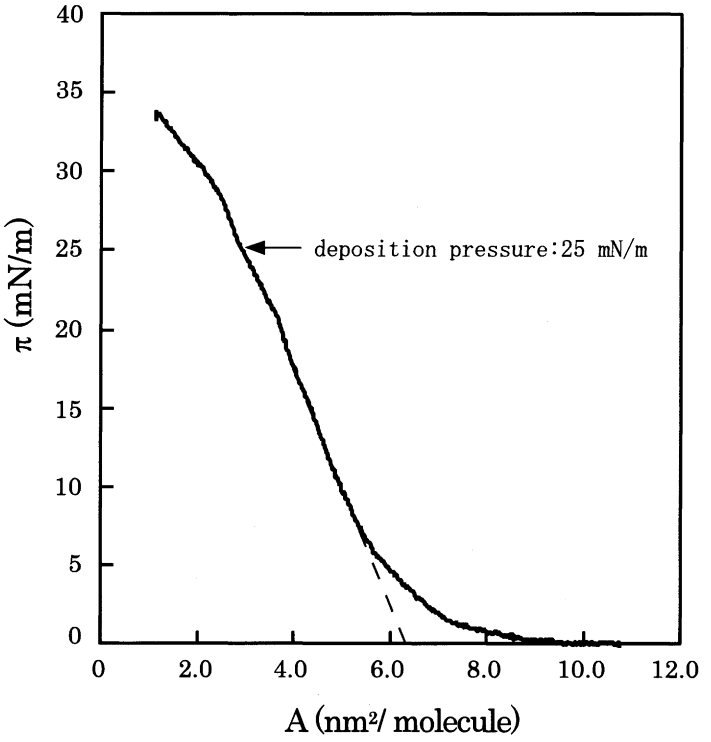

Fig. 7: π–A isotherm for a monolayer of $PLLZ_{25}$–$P(MLG_{42}/LGA_{18})$ with 0.1 mol/l KCl in aqueous solution at pH 5.

Table 1
Limiting area estimated from π–A isotherm.

	Observed (nm^2/molecule) $A_{pH=5}$	Calculated (nm^2/molecule) $A_{\perp}$
$PLLZ_{25}$–$P(MLG_{42}/LGA_{18})$	6.26	2.39

So the monolayer was transferred onto a mica surface at 25 mN/m to get an LB film with a single layer. And the morphology of the LB film was observed by atomic force microscopy (AFM). Fig. 8 shows the AFM image of the LB film on μm scale. From the depth of the cavity that was made by scratching with a cantilever, the thickness of the membrane was estimated to be ca. 1.4 nm. This value is almost consistent with the diameter of the helix, indicating that the α-helix rods lie down on the mica surface. Fig. 9 is a nanometer-scale image of the LB film. A stripe pattern composed of thick and thin layers was observed. And the difference of the thickness was ca. 0.3 nm. This value is almost consistent with the difference between the radii of the hydrophilic and hydrophobic helix rods. This may mean, therefore, that the thick layer is a molecular

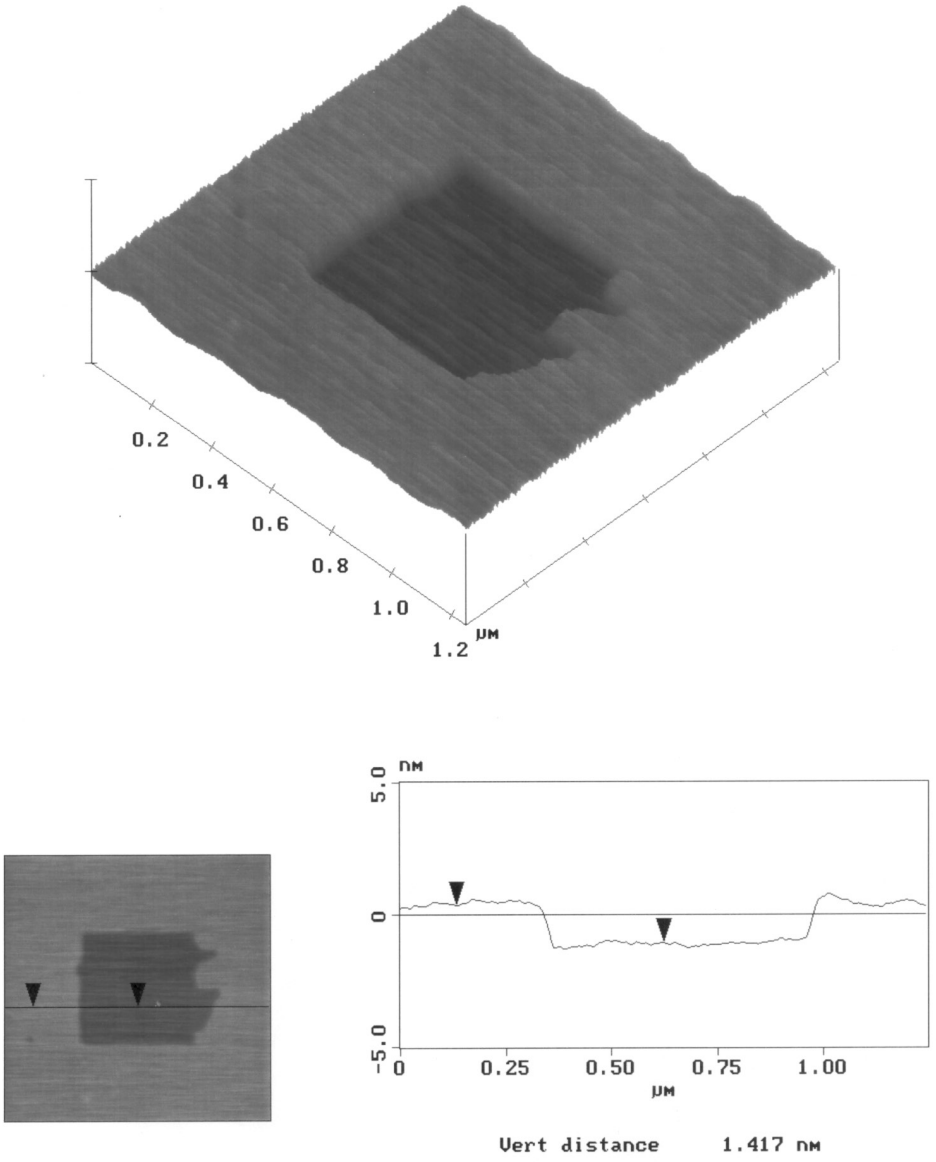

Fig. 8: AFM image (1.25 μm × 1.25 μm) of PLLZ_{25}–P(MLG_{42}/LGA_{18}) LB film on mica (pH 5).

array of the hydrophobic larger-diameter helix and the thin layer that of the hydrophilic smaller helix. The interval of the stripes was estimated to be ca. 24 nm. This value is almost the twice the length of this polymer. These results suggest that this diblock-copolypeptide aggregates by head to head and tail to tail, resulting in the formation of a nanophase-separated structure as is shown in Fig. 10.

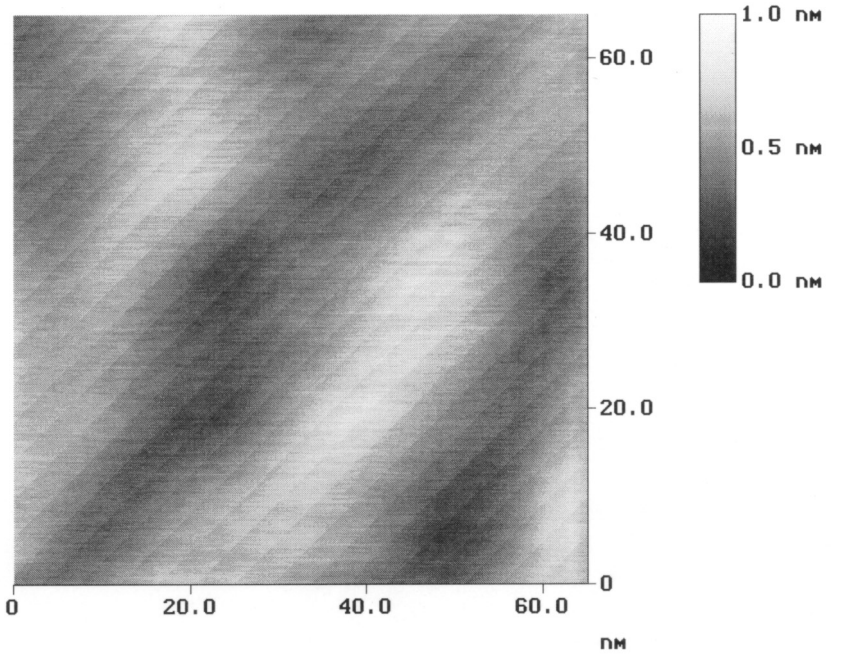

Fig. 9: AFM image (65.1 nm × 65.1 nm) of $PLLZ_{25}$–$P(MLG_{42}/LGA_{18})$ LB film on mica (pH 5).

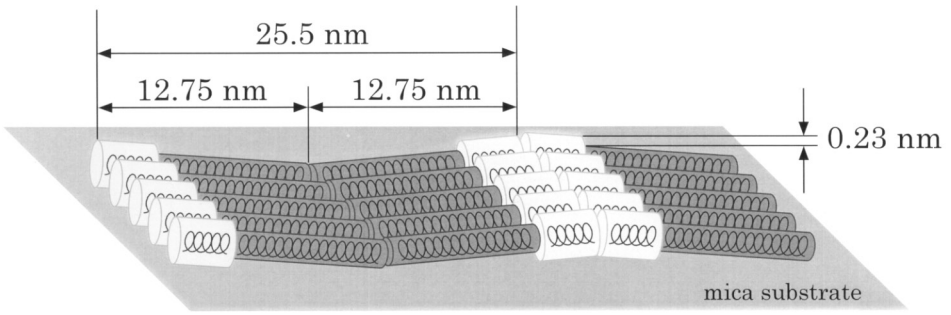

Fig. 10: Schematic illustration of the nanophase-separated structure of $PLLZ_{25}$–$P(MLG_{42}/LGA_{18})$ LB film on mica substrate.

However, Fig. 11(a) is the AFM image within 140 nm^2, a larger area than that of Fig. 9. A disordered structure was observed. That is, except for the regular stripe domain a branching pattern was also made. Fig. 11(b) shows a schematic illustration of the speculated monolayer structure. We think that the hydrophobic interaction and hydrogen bonding between helix rods promote the phase-separated regular pattern, however, the large difference in diameter between the two helix units is not convenient, in this case, for regular packing of the helix rods over a wide range.

So as a next step, the monolayer was prepared by a triblock-copolypeptide composed

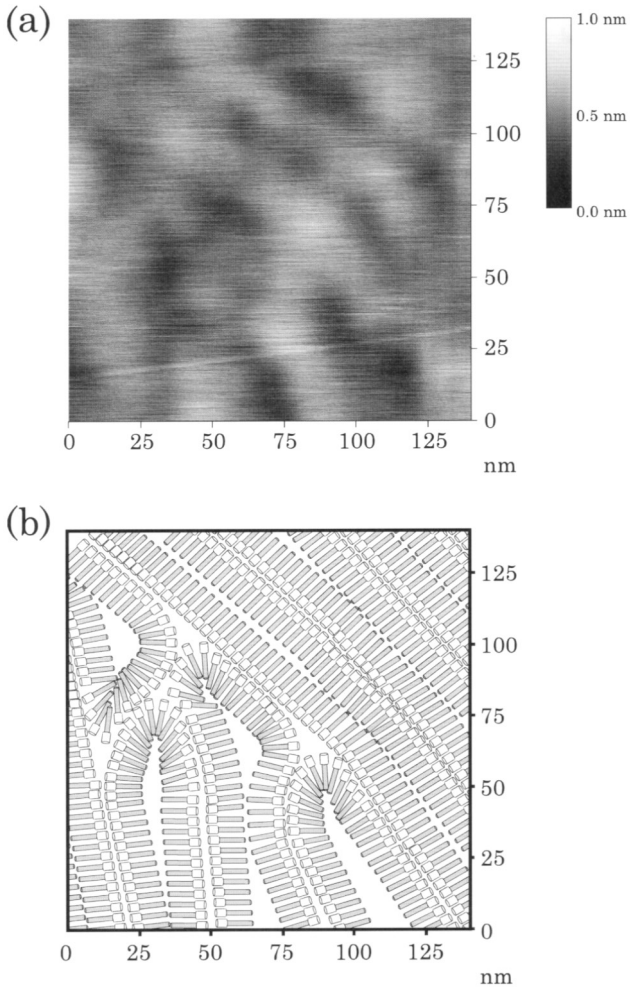

Fig. 11: AFM image (140 nm × 140 nm) of $PLLZ_{25}$–$P(MLG_{42}/LGA_{18})$ LB film on mica substrate (a) and its schematic illustration (b).

of hydrophobic, hydrophilic and hydrophobic helix segments (Fig. 12). We expected that this dumbbell shape will block the development of the branching pattern. The hydrophobic segment is poly(L-leucine) and the hydrophilic segment is poly(L-glutamic acid). The stable α-helix structure was confirmed by FT-IR measurements of the LB film on Au surface. In this case, the monolayer on aqueous solution at pH = 4.0 was transferred on an Au surface for the FT-IR measurements. So this polymer in the acidic condition, as schematically shown in Fig. 12, is composed of a hydrophobic larger-diameter helix and a smaller-diameter hydrophilic helix.

And then, the monolayer on aqueous solution at pH = 4.0 was transferred onto a mica surface to get the LB film with the single layer for AFM measurements. Fig. 13(a)

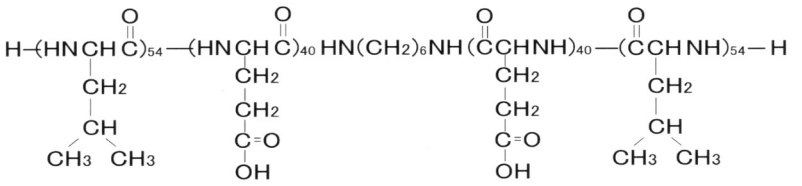

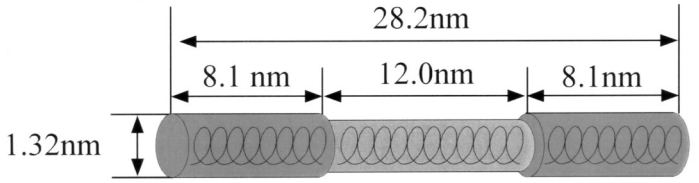

Fig. 12: Chemical structure and schematic illustration of PLL_{54}–$PLGA_{80}$–PLL_{54}.

shows the AFM image of the monolayer within 140 nm^2, indicating a stripe pattern composed of thick and thin layers. The interval of the stripes, in this case ca. 30 nm, is consistent with the length of the triblock-copolypeptide. So, the nanophase-separated structure of the monolayer is schematically shown in Fig. 13(b). As is expected, the triblock-copolypeptide made a more sophisticated stripe pattern with very few branching structures.

We think that this is a good example showing a relation between the molecular shape and character of the polypeptides and their self-organized two-dimensional structure. It is expected, therefore, that the size of this pattern can be regulated by the degree of polymerization of each helix and the functions might be controllable by the side chain structure of the α-helix units.

Thus, we showed the possibility of nanometer-size control of two-dimensional structure for the formation of novel functional interfaces.

3. Two-dimensional structural color formation and regulation using polypeptide LB films

Recently, new types of display systems, such as colored liquid crystal and organic EL (electroluminescence), are rapidly developed and penetrating into our lives as displays of portable telephones, computer games, and displays of sound systems in automobiles. Furthermore, it is expected that the novel display systems should answer the problems of ecology, energy, and human health, especially for the eyes in this case.

It is well-known that nature has unique display systems such as the structural color of butterflies, beetles, and tropical fish and shells. The structural color or interference color, in this case, is based on a nanometer-scale layered structure of the body surface, without any pigments.

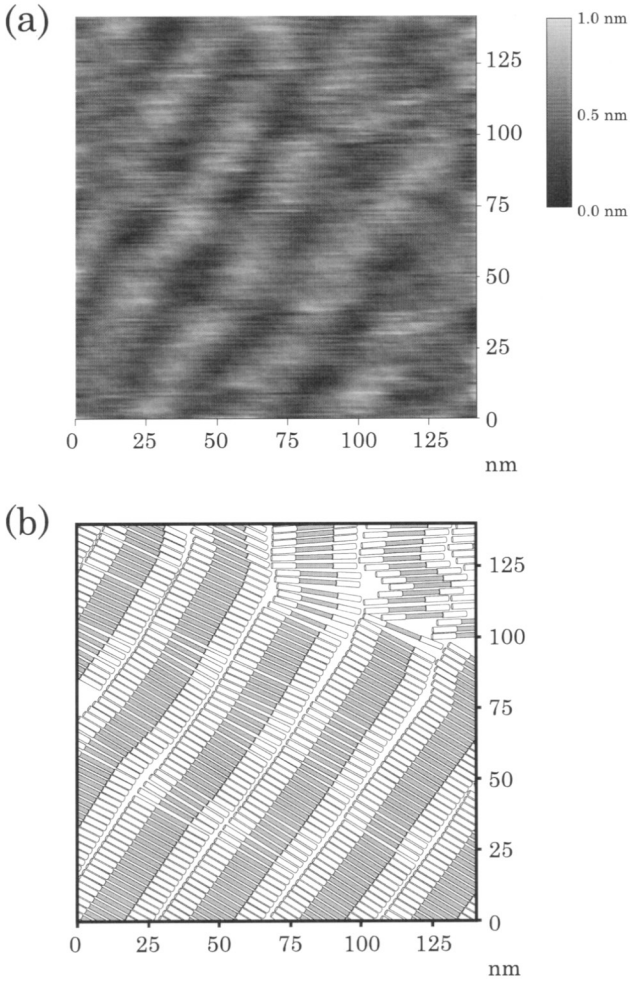

Fig. 13: AFM image (140 nm × 140 nm) of PLL_{54}–$PLGA_{80}$–PLL_{54} LB film on mica substrate (a) and its schematic illustration (b).

When light with a certain incident angle (α) is reflected at the surface layer, it can be emphasized or weakened depending on the wavelength (λ) of the light (Fig. 14). The λ-value of emphasized or weakened light is given by these two equations [6].

$$\lambda = \frac{2h}{m}\sqrt{n^2 - \sin^2\alpha} \qquad \text{(emphasized)} \tag{1}$$

$$\lambda = \frac{4h}{2m-1}\sqrt{n^2 - \sin^2\alpha} \qquad \text{(enfeebled)} \tag{2}$$

where h is thickness of the corresponding layer, n is refractive index of the layer, and m is natural number ($m = 1,2,\ldots$). For α-helix LB films, in our experimental range of $h,m \leq 2$, these two equations can be written as these equations, where d is the diameter

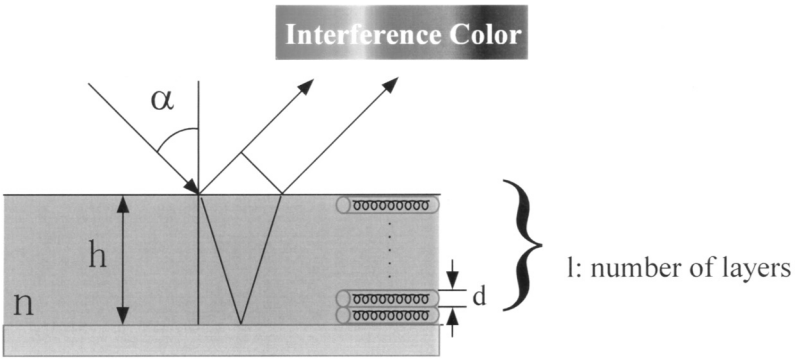

Fig. 14: Principle of structural color formation.

of the helix rod and l is the number of monolayers in the LB film. Thus we can see the particular color from the surface layer according this optical principle.

Structural color materials are also investigated and applied as a color coating technique for ceramic surfaces, such as for example the structural color formation of oxidized titanium [7]. The temperature, in this case, can control the thickness of the oxidized layer and it systematically controls various structural colors. Furthermore, organic materials are also investigated, for example, solution [8] and gel systems [9] for cosmetic application, and structural color fibers are also introduced recently. However, structural color LB systems have not been fully investigated. So recently, we have tried to construct structural color LB films of stimulus–response type as a novel display system [10]. We are using, in this case also, α-helical polypeptide, because the polypeptide can produce a well-defined layered structure on the substrate by the LB method, as we showed above.

The preparation and characterization of polypeptide LB films were investigated by Wegner's group [11–14] using polypeptides with long alkyl side chains (Fig. 15). They call it "hairy-rod". And they showed the supra-molecular structure and optical properties of these LB films, however, did not show the structural color formation.

The long alkyl side chain of polypeptides is easier to crystallize in a film, even at room temperature. This will have a negative influence on the optical properties, so we selected poly(*n*-hexyl L-glutamate) (PHeLG, Fig. 16), which has not so long alkyl chains, as the LB film component. In this case, the stable α-helix conformation of this polymer was also confirmed by CD measurements.

The monolayer was prepared by spreading a DMF/benzene mixed solution of this polymer on a water surface. And the surface pressure was monitored by compressing the monolayer by the Wilhelmy method at 20°C. Fig. 17 shows the surface pressure–area isotherm of this monolayer. The limiting area was estimated to be 26.2 nm^2/molecule. This value is exactly consistent with the calculated limiting area when the helix rod is parallel to the air/water interface. So the monolayer at 15 mN/m was transferred onto a silicon substrate. The substrate is hydrophobized before use by coating a silane-coupling agent with octadecyl moiety and heat-fixed at 110°C. Fig. 18 shows the relation between

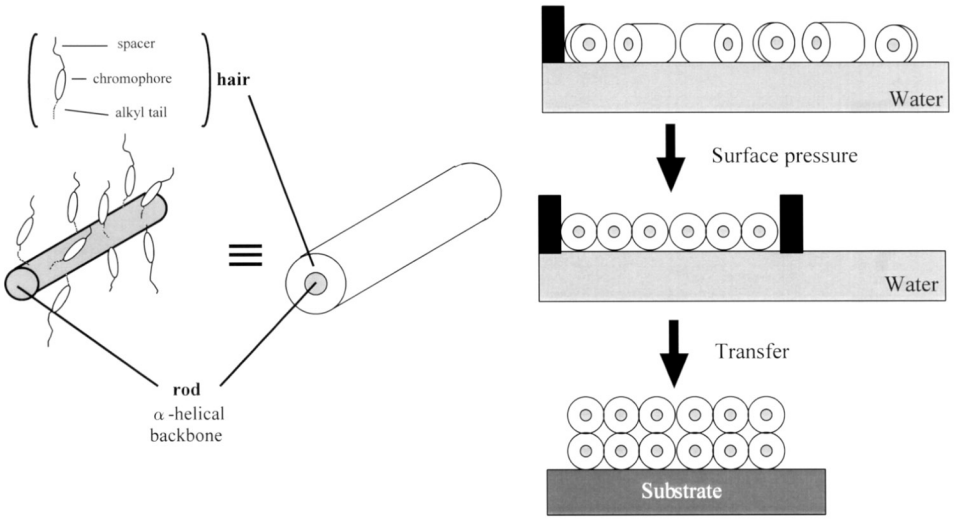

Fig. 15: Schematic illustration of polymer of the "hairy-rod" type, and its orientation on an air/water surface.

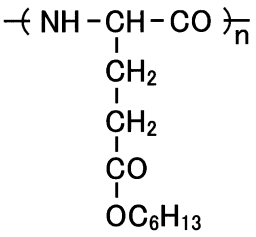

PHeLG

Fig. 16: Chemical structure of poly(*n*-hexyl L-glutamate) (PHeLG).

the deposition ratio and the number of layers. The first step was down mode of the substrate, the second was up mode, and then this repeated alternately. Each deposition ratio is ca. 1, indicating the monolayer was transferred onto the substrate keeping the structure on the water surface.

The structure of PHeLG on the substrate was characterized by FT-IR measurements. Fig. 19 shows a transmission FT-IR spectrum of 120 layers of the LB film. There are four major peaks: a side chain C=O peak, two amide I bands associated with the α-helix structure and the β structure, respectively, and amide II of the α-helix structure. The α-helix amide I band is much larger than that of the β-structure, indicating PHeLG kept the α-helix structure in the LB film after the deposition.

The thickness of LB film on the substrate was measured by AFM. Fig. 20(a) shows an AFM image of the 20 layers LB film with the boundary between the top of the 20 layers and the surface of the substrate itself. The difference in height between them is

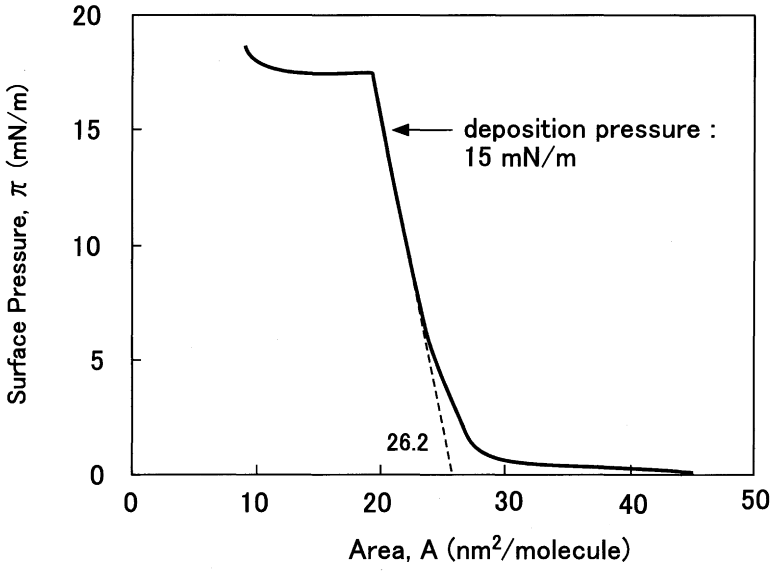

Fig. 17: Surface pressure–area isotherm of PHeLG monolayer at air water interface.

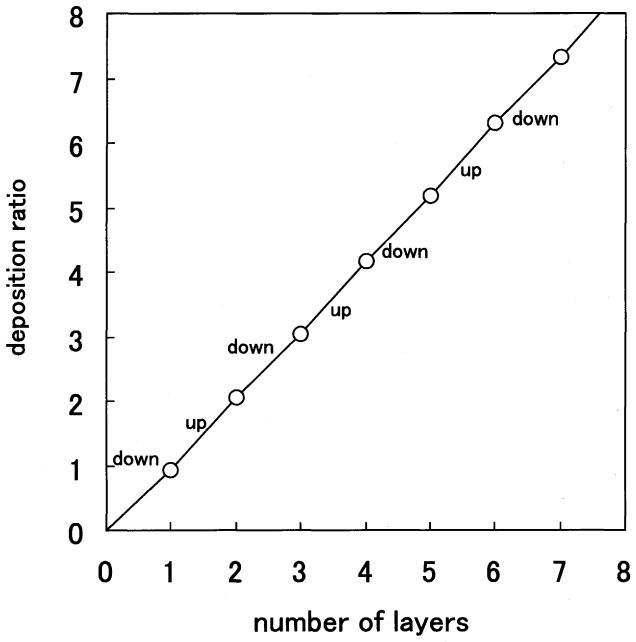

Fig. 18: Deposition ratio of PHeLG monolayer onto silicon substrate as a function of number of layers.

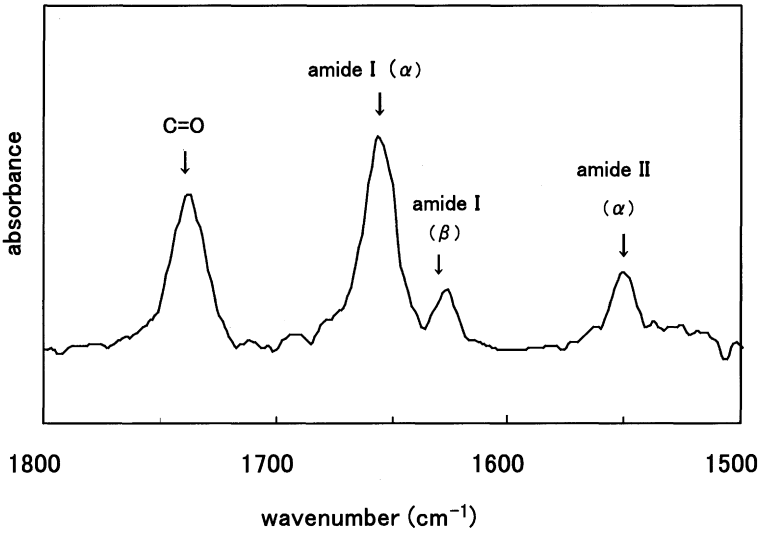

Fig. 19: The transmission FT-IR spectrum of 120 layers of PHeLG LB film.

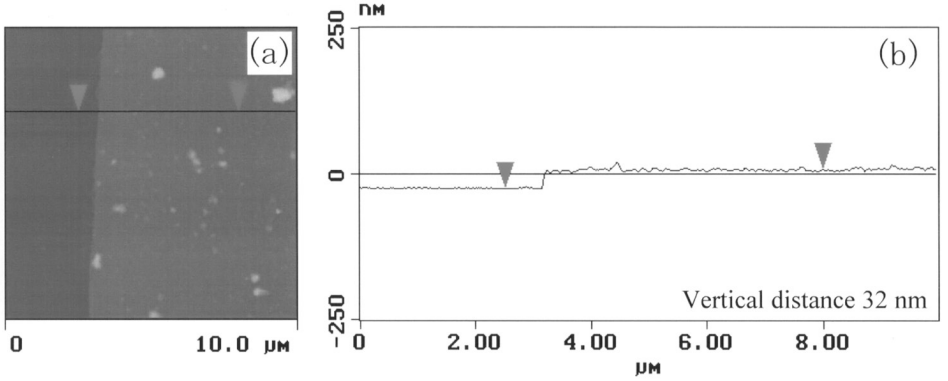

Fig. 20: (a) AFM image of PHeLG LB film; a boundary between 20 layers of PHeLG and the substrate surface. (b) Section of the line in (a).

ca. 32 nm (Fig. 20(b)). This value is corresponding to 20 layers. Therefore, the thickness of one layer is estimated to be ca. 1.6 nm. This value is almost consistent with the diameter (1.5 nm) of PHeLG obtained from the limiting area of the π–A isotherm of this monolayer. Thus, we can confirm a well-defined layered structure in the LB film.

Furthermore, we could find the color formation shown in Fig. 21. The LB films showed various colors depending on the number of layers; brown at 40 layers, dark blue at 80 layers, yellow at 120 layers, and red at 160 layers.

As a next step, the color formation behavior could be quantitatively analyzed by the reflective VIS spectra of these LB films. Fig. 22 shows reflective VIS spectra of the LB films with the incident light angle at 10°. The 80 layers film shows a peak at 418 nm

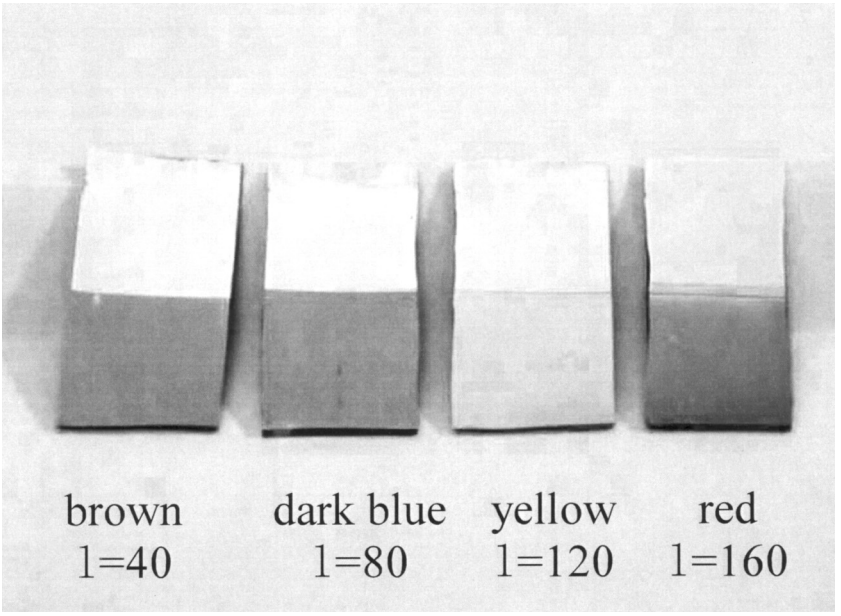

Fig. 21: Structural color of PHeLG LB films.

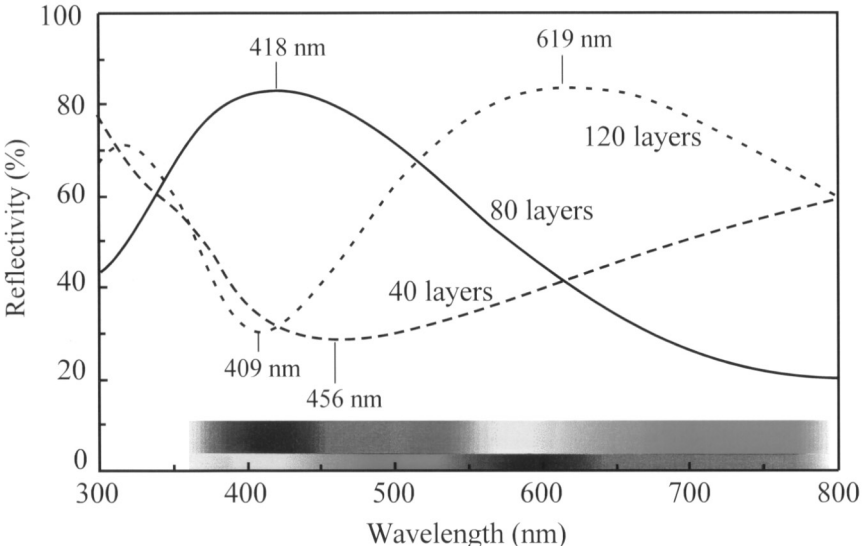

Fig. 22: Reflective VIS spectra of 40, 80, and 120 layers of PHeLG LB films. Incident light angle was 10°.

corresponding to dark blue. Oppositely, the 40 layers film shows a minimum peak at 456 nm corresponding to brown or dark orange which is the complementary color to blue. The 120 layers film shows a peak at 619 nm corresponds to yellow. As a result,

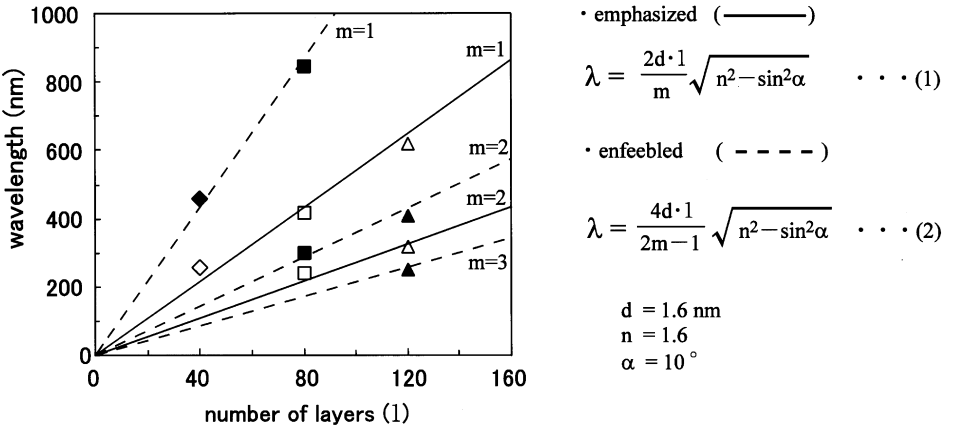

Fig. 23: Measured and calculated wavelength of interference colors as a function of number of layers.

we can compare these peak positions with the calculated values from Eqs. 1 and 2. Fig. 23 shows the measured and calculated wavelengths of colors as functions of number of layers. For example, in the case of 40 layers there is one emphasized peak and one enfeebled peak. And for 80 layers, there are two emphasized peaks and two minimum peaks. The solid lines were obtained by Eq. 1, i.e., λ of the emphasized light, and the dashed lines are λ of the weakened light obtained from Eq. 2, using the parameters ($t = 1.6$ nm and $n = 1.6$). The calculated lines are almost consistent with the measured peaks. Furthermore, Fig. 24 shows observed and calculated peak positions as a function of incident light angle. The open circles and squares are maximum peaks and the filled circles and squares are minimum peaks of these layers, respectively. And the lines A and B were obtained using Eqs. 1 and 2 under the condition A and under the condition B. The condition B yields the same calculated line B. The observed peak positions are almost consistent with the calculated values for all the incident light angles. These results suggest that we can get a structural color forming system by polypeptide-based LB films.

Thus, we obtained a structural color forming system based on the structural modeling approach in Fig. 3. So, we tried to implement stimulus–response coupling functions in our prepared structural color forming system.

First trial is photo-regulation of the structural color. For that, azobenzene containing polypeptides were prepared. It is expected that the photoisomerization of the azobenzene moiety can induce changes in the structure of the LB films (Fig. 25).

This side-chain azobenzene system has been examined. As a result, poly(γ-methyl L-glutamate) containing 28% azobenzene side-chains showed photo-induced changes in the reflective spectrum of the LB film, ca. 10 nm peak shift to lower wavelength. It was also confirmed that the original spectrum can be recovered in the dark.

Fig. 26 shows a shift of the λ_{max} value induced by dioxane vapor sorption, i.e., the solvent-induced swelling of the LB film shifted the λ_{max} to higher value. This is an example of a chemo-responsive structural color forming system. According to the

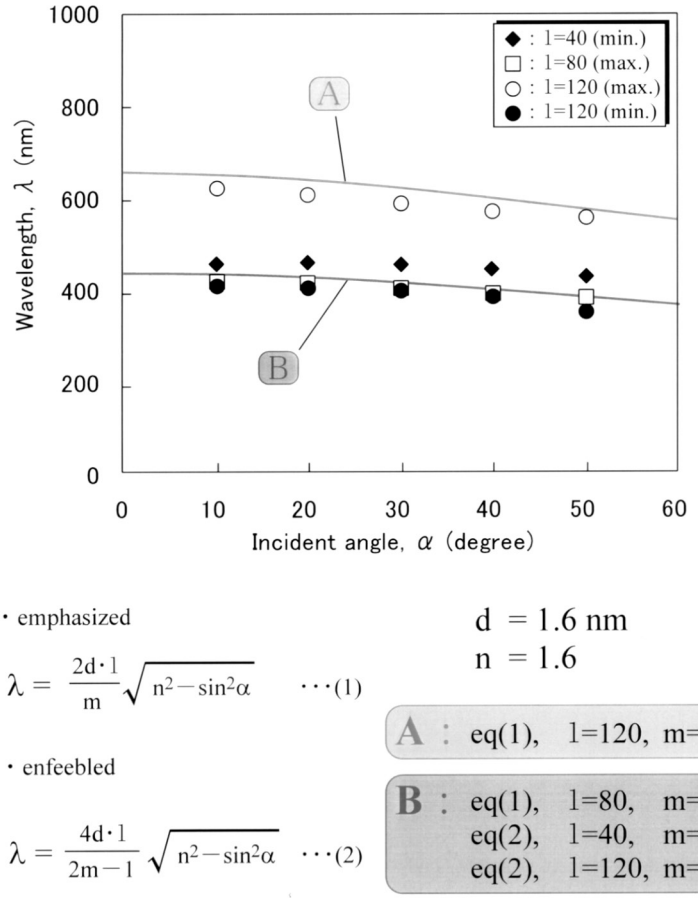

Fig. 24: Measured and calculated wavelengths of interference colors as a function of incident light angle.

evaporation of the solvent during this measurement, this λ_{max} was apparently lowered. So we roughly calculated a shift of λ_{max} using Eq. 1. In this case, the swelling of the layer was estimated by the experimental value of the amount of sorption of dioxane to this LB film, ca. 5% when the relative vapor pressure of dioxane is 0.2 [15]. And the refractive index of the solvent is almost the same as that of the LB matrix. As a result, It was shown that the color should change from the yellow to the red region. We directly observed the color change of the LB film in the sorption chamber. The vapor pressure was controlled by the temperature. As a result, we could observe the expected color change, yellow to pink, thus confirming the solvent-induced color change based on the swelling of the LB film.

On the other hand, methanol shifted λ_{max} to lower wavelength. Opposite to the shift from dioxane. In this case, methanol is a poor solvent, so there is no significant swelling of the layer, so we think that the lower refractive index of the methanol may induce the shift of λ_{max} to lower values.

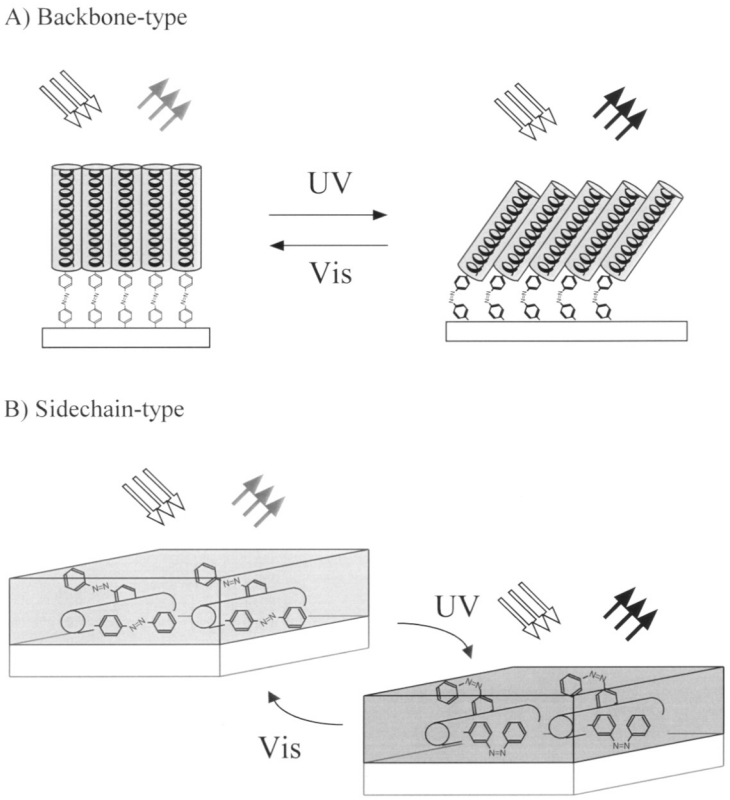

Fig. 25: Control of interference color by azobenzene containing polypeptide LB Films.

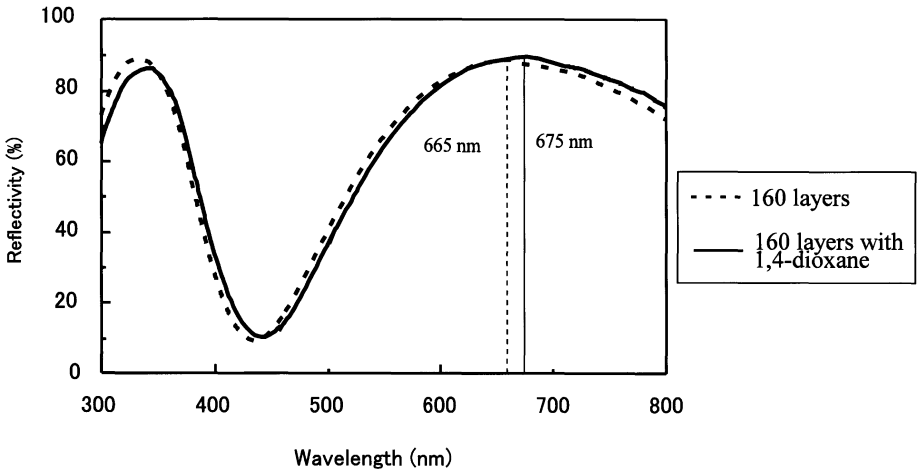

Fig. 26: Reflective VIS spectra of 160 layers of PHeLG LB films on silicon substrate and with 1,4-dioxane. Incident light angle was 10°.

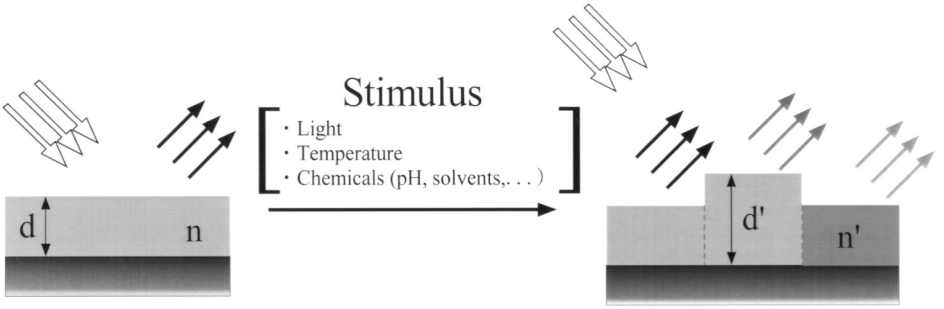

Fig. 27: Control of interference color by stimulus–response coupling.

These results indicate that these LB films sense the chemicals by their color change like litmus paper. We are now trying to construct such stimulus–response LB films using light, temperature and chemicals as a stimulus (Fig. 27). This type of novel display and novel sensing system will be more sophisticated in 1–2 years, based on the fundamental results today.

Acknowledgements

This study has been supported by the New Energy and Industrial Technology Development Organization (NEDO), Japan, for the project on Technology for Material Structure Control.

References

1. S.J. Singer and G.L. Nicolson, Science, **175**, 720 (1972).
2. Y. Miura, S. Kimura, Y. Imanishi, and J. Umemura, Langmuir **14**, 6935 (1998).
3. N. Higashi, T. Koga, Y. Fujii, and M. Niwa, Langmuir **17**, 4061 (2001).
4. T. Kinoshita, Prog. Polym. Sci. **20**, 527 (1995); J. Photochem. Photobiol. B **42**, 12 (1998).
5. H. Yokoi, T. Kinoshita, Y. Tsujita, and H. Yoshimizu, Chem. Lett., 1210 (2000).
6. E. Hecht and A. Zajac, *Optics* (Addison-Wesley, Reading, MA, 1974).
7. S. Sakka, K. Kamiya, and T. Yoko, *ACS Symposium Series 360* (American Chemical Society, Washington, DC, 1988) pp. 345–353.
8. K. Naitoh, Y. Ishii, and K. Tsujii, J. Phys. Chem. **95**, 7908 (1991).
9. M. Hayakawa, T. Onda, T. Tanaka, and K. Tsujii, Langmuir **13**, 3595 (1991).
10. T. Kinoshita, S. Hayashi, and Y. Yokogawa, J. Photochem. Photobiol. A **145**, 101 (2001).
11. G. Duda, A.J. Schouten, T. Arndt, G. Lieser, G.F. Schmidt, C. Bubeck, and G. Wegner, Thin Solid Films **159**, 221 (1988).
12. W. Hickel, G. Duda, M. Jurich, T. Kröhl, K. Rochford, G.I. Stegeman, J. D. Swalen, G. Wegner, and W. Knoll, Langmuir **6**, 1403 (1990).
13. A. Mathy, K. Mathauer, G. Wegner, and C. Bubeck, Thin Solid Films **215**, 98 (1992).
14. M. Büchel, Z. Sekkat, S. Paul, B. Weichart, H. Menzel, and W. Knoll, Langmuir **11**, 4460 (1995).
15. T. Kinoshita, N. Okazaki, A. Takizawa, and Y. Tsujita, Polymer **20**, 791 (1979).